Structural review of PPARγ in complex with ligands: Cartesian- and dihedral angle principal component analyses of X-ray crystallographic data.

Åsmund Kaupang,[a,*] Tuomo Laitinen,[b] Antti Poso[b] and Trond Vidar Hansen.[a]

[a]Department of Pharmaceutical Chemistry, School of Pharmacy, University of Oslo, P.O. Box 1068, Blindern, 0316 Oslo, Norway.

[b]Department of Pharmaceutical Chemistry, School of Pharmacy, University of Eastern Finland, P.O. Box 1627, Kuopio, Finland.

[*]Corresponding author. Tel.: +47 22 85 44 78; e-mail: asmund.kaupang@farmasi.uio.no

The work was carried out at both the above mentioned institutions.

Short title: Structural review of PPARγ-ligand complexes.

Keywords: PPARγ, structure, database analysis, principal component analyses, ligand-induced stabilization, helix 12, structure mapping.

Abbreviations: cPCA, Cartesian (coordinate) principal component analysis; dPCA, dihedral angle principal component analysis; FRET, Förster/fluorescence resonance energy transfer; HDX-MS, hydrogen-deuterium exchange coupled to mass spectrometry; LBD, ligand-binding domain; LBP, ligand-binding pocket; MD, molecular dynamics; NMR, nuclear magnetic resonance; PPARγ, peroxisome proliferator-activated receptor γ.

Abstract (strict 250 word limit)

Two decades of research into the ligand-dependent modulation of the activity of the peroxisome proliferator-activated receptor γ (PPARγ) have produced a large body of structural data from single-crystal X-ray diffraction studies of PPARγ in complex with a diverse set of ligands – among them several drugs in clinical use. The heterogeneous modes of action observed among PPARγ ligands in terms of their interaction surfaces in the ligand-binding pocket, their binding stoichiometry and their utilization of allosteric stabilization mechanisms, complicate an explanation of their transcriptional effects. Consequently, a collective analysis of the PPARγ X-ray structures available in the public domain, focusing on ligand-induced structural trends, is in demand. Herein, principal component analyses of the atomic (Cartesian) coordinates (cPCA) and dihedral angles (dPCA) are applied to this ensemble of structures. In the cPCA, projections of the structures along the extracted principal components (PCs) demonstrated a moderate correlation between the cPC1 and structural parameters that are central to the transcriptional regulation by PPARγ, such as the stabilization of helix 12. Thus, the mapping of the PPARγ-ligand complexes from the cPCA may be applied in drug discovery programs seeking to avoid stabilization of helix 12 in their development of new partial- and non-agonistic PPARγ ligands. The dPCA provided an intriguing separation of the PPARγ structures into distinct clusters, improving upon the separation observed along cPC2. While the clusters identified key regions of dihedral fluctuation in the ensemble, they could not be differentiated according to the same structural parameters as the cPC1 distribution.

Introduction

The peroxisome proliferator-activated receptor γ (PPARγ) is a transcription factor regulating the expression of genes involved in lipid storage and glucose expenditure,[1] but also in kidney function,[2] bone metabolism[3] and neuronal development.[4] It is the most well-studied member of the PPAR family of nuclear receptors and both ligand-dependent and ligand-independent modes of modulation of its activity have been established. Among these, the ligand-dependent modulation of PPARγ activity has been a major focus in commercial and academic drug discovery programs seeking new treatments for human metabolic diseases, such as type II diabetes mellitus and metabolic syndrome.[1] More recently, the role of PPARγ in neurodegenerative disease has received increased attention.[4,5]

Research efforts from the past two decades have produced an array of small-molecular modulators of PPARγ, whose beneficial effects on e.g. insulin sensitivity, have allowed the application of members of the thiazolidinedione (TZD) family of PPARγ agonists in a clinical setting. In parallel, however, a body of evidence has grown, describing class-wide side effects of the TZDs, such as fluid accumulation (edema),[2] increased risk of heart failure[6] and decreased bone density.[7] The origin of these side effects was recontextualized by the discovery of a ligand-sensitive, post-translational modification (PTM) of the PPARγ ligand-binding domain (LBD) (Figure 1). In 2010, Choi et al. demonstrated that the ligand-dependent inhibition of a phosphorylation of Ser273 (Ser245 in PPARγ1 numbering, which is used throughout this text) by cyclin-dependent kinase 5 (Cdk5), led to the regularization of the expression levels of a set of genes known to be dysregulated in obesity (including adipsin and adiponectin). Importantly, it was shown that this gene set was only a subset of the genes whose expression was regulated by the treatment of PPARγ with the TZD rosiglitazone (**1**) (Figure 2). Furthermore, the ligand

MRL24 (**2**) inhibited phosphorylation of Ser245 (Ser273) as efficiently as rosiglitazone (**1**), even though **2** is a weak agonist compared to **1**, in assays measuring the transcription of chimeric PPARγ reporters or classical, adipogenesis-related PPARγ target genes.[5] By X-ray crystallographic analysis, hydrogen-deuterium exchange coupled to mass spectrometry (HDX-MS) and nuclear magnetic resonance (NMR) spectroscopy, MRL24 (**2**) has been shown to preferentially bind to a different site in the PPARγ ligand-binding pocket (LBP) from both its regioisomer, the potent agonist MRL20 (**3**) and rosiglitazone (**1**). In its binding mode, MRL24 (**2**) did not stabilize the PPARγ C-terminal helix 12 (shown in orange, Figure 1).[5,8,9] This helix is central to the nuclear receptor activation function 2 (AF2) and to the formation of a surface binding groove for transcriptional coactivator proteins.[10] The LBP interaction patterns observed for MRL24 (**2**) versus MRL20 (**3**), which does stabilize helix 12, were thus coherent with the lower transcriptional activation observed upon treatment of PPARγ with 2. Conversely, MRL24 (**2**) stabilized the β-sheet region in the Ω-pocket (shown in yellow, Figure 1), which in turn stabilized the external loop containing Ser245, making it less available for Cdk5-mediated phosphorylation.[5,8,11] Recently, it was shown that a second molecule of MRL20 (**3**) can bind to the Ω-pocket, simultaneously with the AF2-pocket being occupied by **3** or blocked by covalent antagonists, targeting Cys285. Both double occupancy of the LBP, as well as binding to the Ω-pocket alone were demonstrated to allosterically influence transcriptional regulation by PPARγ.[9]

Among the reported PPARγ modulators that display weak transcriptional induction, is also the ligand SR1664 (**4**) (Figure 2). Intriguingly, its *R*-enantiomer SR1663 (**5**) is a potent PPARγ agonist. While **4** and **5** can display nearly identical binding modes, in which both interact with the β-sheet region through their carboxylate groups, but stretch around helix 3 and into the Ω-pocket, where they differ in their interaction with Phe282 (PDB ID: 4r2u and 4r6s).[12] In the

case of SR1664 (**4**), this interaction near completely attenuates the transcriptional induction by PPARγ, likely through a destabilization of helix 12.[12,13] A later crystallographic study revealed that SR1664 (**4**) can also assume an alternative binding mode in which it no longer occupies the AF2-pocket. In this structure, **4** is located in the Ω-pocket where it interacts with helix 3 and the Ω-loop (PDB ID: 5dwl).

The above presented examples of structurally related ligands with highly divergent transcriptional effects demonstrate the diverse nature of ligand binding in the PPARγ LBP, in which multiple binding sites, ligand stoichiometry and allosteric communication between subpockets must be taken into account. The second example also demonstrates how ligand presence in the AF2-pocket is not necessarily conducive to transcriptional activation, if the ligand, directly or indirectly, causes a perturbation of helix 12.

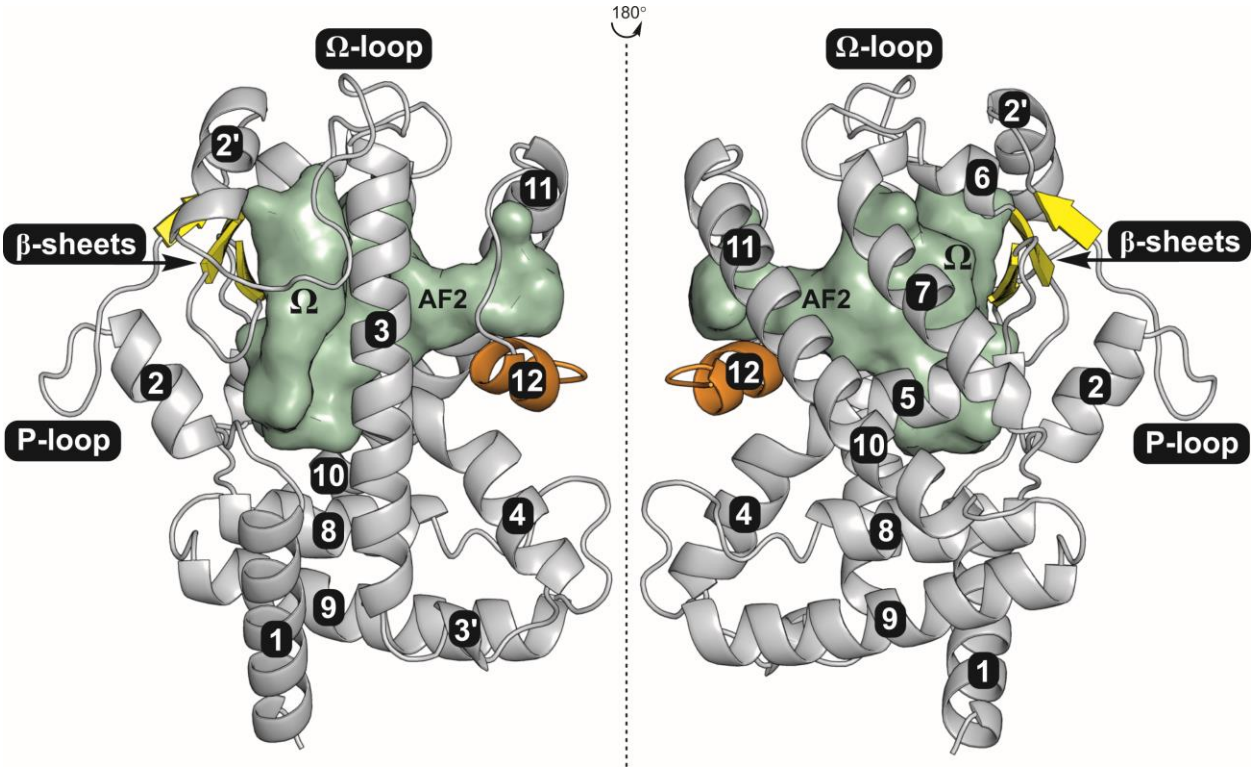

Figure 1. The overall structure of apo-PPARγ with numbered helices and loops. In the left view, the pocket regions neighbouring the β-sheets (yellow) and helix 12 (orange), are marked as the Ω-pocket and the AF2-pocket, respectively. The LBP surface was generated with HOLLOW[14] and the apo-PPARγ structure (PDB ID: 2zk0, chain A) was visualized with PyMOL.[15]

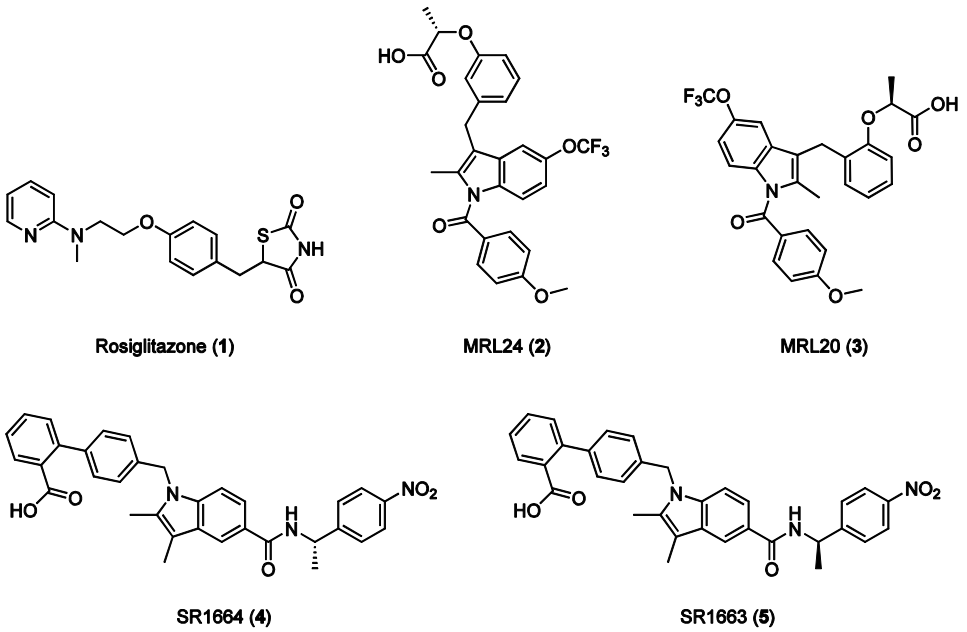

Figure 2. Chemical structures of the PPARγ agonists rosiglitazone (**1**), MRL20 (**3**) and SR1663 (**5**), as well as the partial- and non-agonists MRL24 (**2**) and SR1664 (**4**). The structures are drawn in 2D-orientations reminiscent of their 3D-poses in PPARγ, when viewed as depicted in Figure 1 (left).

Examples of other ligands that display binding to the Ω-pocket in the PPARγ LBP, include fatty acids of certain lengths, fatty acid metabolites, serotonin metabolites, phenolic natural products, as well as various synthetic partial agonists, including several non-steroidal anti-inflammatory drugs (NSAIDs).[11,16–21] The data describing the binding modes of these ligands, as well as those of classical agonists, largely stem from X-ray crystallographic studies. Collectively, these data demonstrate the ability of PPARγ to bind ligands in diverse poses and ligand stoichiometries (Table S1 in the Supporting Information for examples). On the other hand, the impacts on the dynamics of the PPARγ LBD resulting from the binding of these classes of ligands, have been studied with techniques such as HDX-MS, NMR spectroscopy and molecular dynamics (MD) simulations.[8,9,11,22–24] Together, these investigations have provided insights into the differential stabilization of specific regions of the PPARγ LBD in response to the binding of these ligands, e.g. helix 3, the β-sheet region, and the P- and Ω-loops (Figure 1). They have also established that ligands binding to the Ω-pocket may allosterically stabilize helix 12 through residue networks e.g. in the Ω-loop and on helix 3.[9,12,16,25,26] Finally, for several of the ligands, FRET-based measurements of the affinity of the PPARγ-ligand complexes for fluorescently labelled peptides derived from transcriptional coregulator proteins, offer ligand-specific coregulator interaction profiles.[9,27–29] Such profiles create bridges between the structural realm and the ligand-dependent variations observed in the transcription of PPARγ target genes.

Given the diverse set of ligands with which PPARγ has been cocrystallized, an evaluation of the sampled conformational space using PCA could potentially provide novel insight into collective structural differences between the PPARγ complexes with the partial- and non-agonistic ligands, and those with classical agonists. A relative classification of these complexes could add to our understanding of the different modes of ligand-dependent PPARγ activation.

While in a dynamical sense, these ligands may be envisioned to contribute to populational shifts between PPARγ conformational ensembles, possibly already present in the apo-state,[22,30–32] the degree to which these influences are present in the crystal phase is less well understood. Aiming to shed light on these questions, we evaluated the correlations between the distributions of the structures projected on to the principal component axes, and PPARγ structural parameters or ligand functional attributes.

Theoretical Basis. Principal component analysis (PCA) is a ubiquitously applied technique for extracting the principal directions and magnitudes of the variance in a dataset. PCA involves a transformation of a given dataset into a new coordinate system, in which the direction of largest variance in the dataset becomes the axis of the first principal component, PC1. The direction of the second largest variance becomes the axis of the second principal component, PC2, etc. The resulting axes, PC_n, are necessarily orthogonal. The new coordinate system is thus unique to each dataset, as the dataset variances define its axes.[33] An expressed limitation of classical PCA when it comes to the biophysical relevance of the patterns of variance it can extract, concerns the projection of the dataset variance onto linear, orthogonal axes. The variances produced by protein functional dynamics may not be optimally captured in terms of linear correlations.[34,35] Notwithstanding this, the application of PCA to biological structural data, also known as essential dynamics analysis (EDA),[35] has been used to extract key modes of protein motion. The results of these analyses have been coherent with data from other analytical techniques, and have thus contributed to the elucidation of the functional mechanics of the studied proteins.[36–42]

Classically, in PCA of protein structural data, the variances of the Cartesian coordinates of a macromolecular system are analyzed (hereafter referred to as cPCA).[36–38] Other bases of data, such as the fluctuations of the dihedral angles of the protein backbone may also be transformed with PCA. This transformation is less straightforward due to the circular nature of dihedral angles, in which e.g. angles of -179º and 179º, that are similar in physical space, produce an arithmetic mean of 0º, instead of ±180º. Nevertheless, through the representation of each dihedral angle as sine/cosine pairs, dihedral angle principal component analysis (dPCA) as introduced by Stock et al., has demonstrated that it can capture the potential energy surfaces visited in peptide folding simulations with intriguing detail.[39–42] The challenges inherent to the use of dihedral angles in PCA have also been tackled in an alternative approach, employing principal component geodesics, named GeoPCA.[43]

Materials & Methods

LBP Surface Generation. The LBP surface shown in Figure 1 was generated with HOLLOW,[14] which traces the interior surface of the LBP by filling it with spheres on a 0.5 Å grid. The resulting surface and the PPARγ structure (PDB ID: 2zk0, chain A) were visualized with PyMOL.[15]

Dataset Characteristics. The PPARγ structural data was obtained from the PDB_REDO databank.[44,45] which contains optimized and consistently refined entries from the RCSB Protein Data Bank.[46] The X-ray crystallographic data of PPARγ available in the public domain, per January 2017, comprise 155 entries, of which 134 were deemed suitable for the initial analyses, excluding point mutants, structures whose data were recorded at temperatures other than 100±10

K and structures without deposited structure factors. The latter exclusion criterion arose from the choice to obtain the X-ray crystallographic data from the PDB_REDO server.[44,45] In the suitable structures the asymmetric units contain PPARγ as a dimer, either with another PPARγ protein or with RXRα. There are also examples of PPARγ tetramers and monomers. Some of the structures also include oligopeptides derived from the nuclear receptor-binding motifs of coactivator proteins (typically from SRC-1).

Utilized Software and Data Treatment. The PDB-files were parsed with the functions implemented in the Python software package ProDy (ver. 1.6.1),[47] which was used for the cPCA calculations. ProDy was also used for producing a PDB-file of the reference structure (apo-PPARγ, PDB ID: 2zk0, chain A) accompanied by an ordered pseudo-trajectory of the structural ensemble in DCD-format. The Visual Molecular Dynamics (VMD) software (ver. 1.9.1)[48] was used to parameterize the protein topology (CHARMM36 version, July 2012)[49] in the reference structure PDB-file and to output this structure in PSF-format. The PSF- and DCD-files were then used as inputs for the software Carma (ver. 1.4),[50,51] which performed the dPCA. The numerical results were read back into Python and plotted using standard Python plotting functions (matplotlib, ver. 1.3.1). An in-house program written in Python was used to coordinate the efforts of the above mentioned softwares (Python, ver. 2.7.6).[52] This code is available from the corresponding author upon request.

Analyzed Residue Selection. For the principal component analyses, the heavy atoms of the protein backbone (N, C_α, C, O) of the PPARγ LBD (residues 207 – 477) were used. The mobilities of parts of the P-loop (residues 239 - 244), most of the Ω-loop (residues 259 – 275) and the three C-terminal residues (475 - 477) are high and only resolved in part of the dataset. The residue selection was thus limited to the residues resolved in most of the structures, in order

to achieve consistent occupancies in the analyzed datasets. The minimum occupancies of the residue selections used in the described PCAs were: 76.4% for the calculations of Figures 3A and 3B, 95.3% for the calculations in Figures 3C and 3D and 95.4% for all calculations on the final dataset (PPARγ:PPARγ homodimers, *vide infra*).

Plotting and Structure Mapping. The plots of the distributions obtained from PCA display the analyzed structures projected along PC1 - 2. In these plots, each structure (datapoint) is coloured according to structural parameters or parameters relating to their bound ligand(s), as explained in the legend of each plot. Herein, only the first two principal components (PC1-2) from the analyses are shown and discussed, as these represent the largest variances in the dataset and since trends similar to those observed along PC1-2 (*vide infra*) were not found among the higher PCs. dPC1-2 were also the only dPCs that displayed multipeak distributions. Finally, aiming to provide a useful reference for other workers, the distributions along PC1/PC2, from the cPCA and dPCA of the final dataset, are presented with numbered datapoints in Figure S1 in the Supporting Information. The PDB IDs corresponding to these numbers are listed in Table S2.

Results & Discussion

Initial Analyses of the Dataset. Initially, the entire dataset was analyzed (237 PPARγ structures from 134 entries). As can be seen in Figure 3A, a projection of these structures onto the first two principal components of the cPCA (cPC1 and cPC2), distinguishes two large clusters. These two clusters correspond to the two general conformers of PPARγ, commonly observed by X-ray crystallographic analysis. The most pronounced structural difference between these conformers, often referred to as type A and type B chains, lies in the observed position of helix 12. In the type

A chains (Figure 3A, left cluster), helix 12 is located in the canonical active position,[53] covering one of the entrances to the LBP and positioned roughly orthogonally to helix 3 (Figure 1). In the type B chains (Figure 3A, right cluster), helix 12 is retracted towards the groove between helix 3 and helix 11, to a position that is roughly parallel to helix 3 (Figure S2 in the Supporting Information). cPC1 and cPC2 explain 75.9% and 5.2% of the dataset variance, respectively (cPC1 - 5, 87.2%). The dPCA provides less distinction between these two types of chains (Figure 3B), a result which likely reflects the large numerical magnitude of the variance between type A and type B chains in the positional data (Cartesian coordinates), compared to that in the dihedral angle data.

The two homodimeric structures of apo-PPARγ (PDB IDs: 1prg and 2zk0) included in this analysis both present type A and type B chains. The origin of the type B chains, which are frequently more poorly resolved in the crystals than the type A chains, have received little detailed treatment in the literature of the published X-ray structures, and their relative position of helix 12 has earned them a status as "inactive". In this context, a solution NMR study of apo-PPARγ by Johnson et al. observed two distinct amide N-H chemical shifts for Tyr473.[22] Several NMR studies have found that a large number of crosspeaks missing from the spectra of apo-PPARγ, are partially to fully restored upon addition of a ligand.[8,22,23,54] These findings attest to apo-PPARγ being a highly mobile structure in solution, whose conformational population is focused upon ligand binding. Both the larger conformational freedom of helix 12 in apo-PPARγ, as well as its two main conformers were recently been reproduced by MD simulations.[32]

86 of the 110 structures containing PPARγ homodimers display type B chains, which could suggest that the observation of a type B chain in the crystal phase stems from the presence of type B chain-like structures in the conformational ensemble of PPARγ in complex with a given ligand.[55] However, as suggested by Johnson et al., the observation of two distinct conformations of helix 12 in the crystal phase, may also owe to a specific stabilization of these two conformers by the crystal packing.[22] Which is the dominant of these effects is unclear, particularly as helix 12 itself is involved as a lattice contact in the crystal packing of the PPARγ homodimeric structures. Interestingly, in these structures, helix 12 of the type B chains is positioned roughly in the coactivator groove of the type A chains. In summary, a more complete understanding of the role of PPARγ conformers similar to the type B chains requires further study. This, in combination with the inconsistent ligand occupancy of the type B chains, encouraged us to focus our analyses on the type A chains.

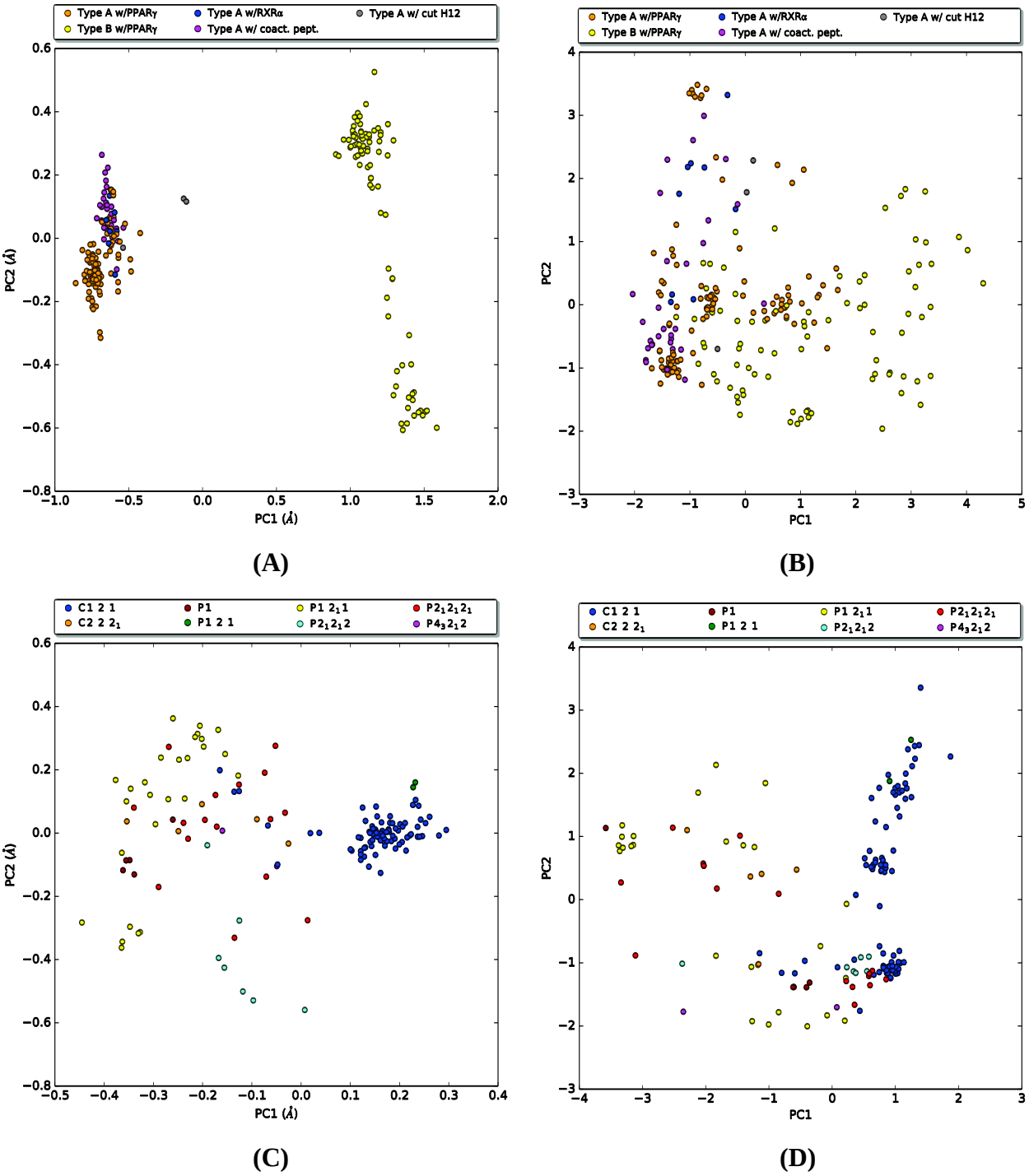

Figure 3. *Top:* cPCA (**A**) and dPCA (**B**) of all PPARγ structures in the dataset coloured according to their eventual dimeric partners or cocrystallized peptides. *Bottom:* cPCA (**C**) and dPCA (**D**) of all type A chains in the dataset coloured according to their crystallographic space groups.

The crystal environment, may exert a significant influence on the structural data, that in turn may skew a comparative analysis of the same protein across crystals.[56–58] Factors related to the crystallization conditions, including the presence of salts, surfactants or other additives in the crystallization buffers, endogenous ligands from protein expression systems, as well as the often recombinant nature of the PPARγ LBD itself, all influence the crystal packing. Aiming to evaluate the dependence of the structural data on these parameters, the structures of the PPARγ type A chains were projected onto their first two principal components and coloured according to their crystallographic space groups. As can be seen in Figures 3C and 3D, the crystal packing impacts on the structural data and the tightest cluster observed along cPC1 and cPC2 is reasonably well explained by its members having crystallized in the C 1 2 1 space group. cPC1 also provides some separation of the structures in the space groups P 1 2_1 1 and P 2_1 2_1 2_1. cPC1 and cPC2 explain 21.1% and 12.3% of the dataset variance, respectively (cPC1 - 5, 53.5%). The dPCA also expresses correlations between the distributions of the structures and their crystallographic space groups, but provides less separation, except in the case of the structures in the C 1 2 1 space group. On the other hand, the tendency for a protein-ligand complex towards a given crystal packing and -symmetry is also influenced by the stabilization of the protein by the ligand. Consequently, the correlation between the observed distributions of the holo-PPARγ structures and their respective crystallographic space groups, may not be void of information regarding the effects of their bound ligands. Nonetheless, due to the general heterogeneity of the dataset with regards to their crystallographic space groups, dimeric partners and the presence of coactivator peptides, the remaining analyses focus on the type A chains of the PPARγ homodimeric structures (86/149 structures with type A chains), nearly all of which crystallized in the C 1 2 1 space group. This dataset had an average resolution of 2.32 Å (1.77 – 2.90 Å).

Analyses of a Focused Dataset. With this dataset, the distribution along dPC1 – 2 provided a clearer separation of the structures than that along cPC1 - 2. By colouring the three main clusters seen in Figure 4B and transferring these colours back to the distribution along cPC1 – 2 (Figure 4A), it becomes apparent that cPC2 indeed differentiates the structures in a manner similar to dPC1, although less distinctively. While only the distributions along dPC1 – 2 display obvious multipeak behaviour, the distributions along cPC1, cPC2, dPC1 and dPC2 are all non-normal, indicating that they are not likely to have been drawn from random populations. This, in turn, supports the notion that they contain relevant structural information (Figure S3 in the Supporting Information for more details on normality testing).[59,60] cPC1 and cPC2 explain 20.2% and 14.2% of the dataset variance, respectively (cPC1 - 5, 52.8%).

Structurally, cPC1 describes a correlated lifting motion of the end of helix 11 and of helix 12. Motions of smaller magnitudes that are anti-correlated to this lifting motion are seen in end of helix 6 and beginning of helix 7, as well as in helix 2' (Supporting Movies 1 - 3). cPC2, on the other hand, describes flipping and stretching motions in the end of helix 11 and of the loop preceding helix 12, as well as in the loop between helix 6 and helix 7. It also describes a wagging motion of helix 2' that is orthogonal to the motion described by cPC1 (Supporting Movies 4 – 6). In summary, cPC1 – 2 appear to capture differences between the analyzed structures that involve regions of PPARγ known to be important for its transcriptional regulation.

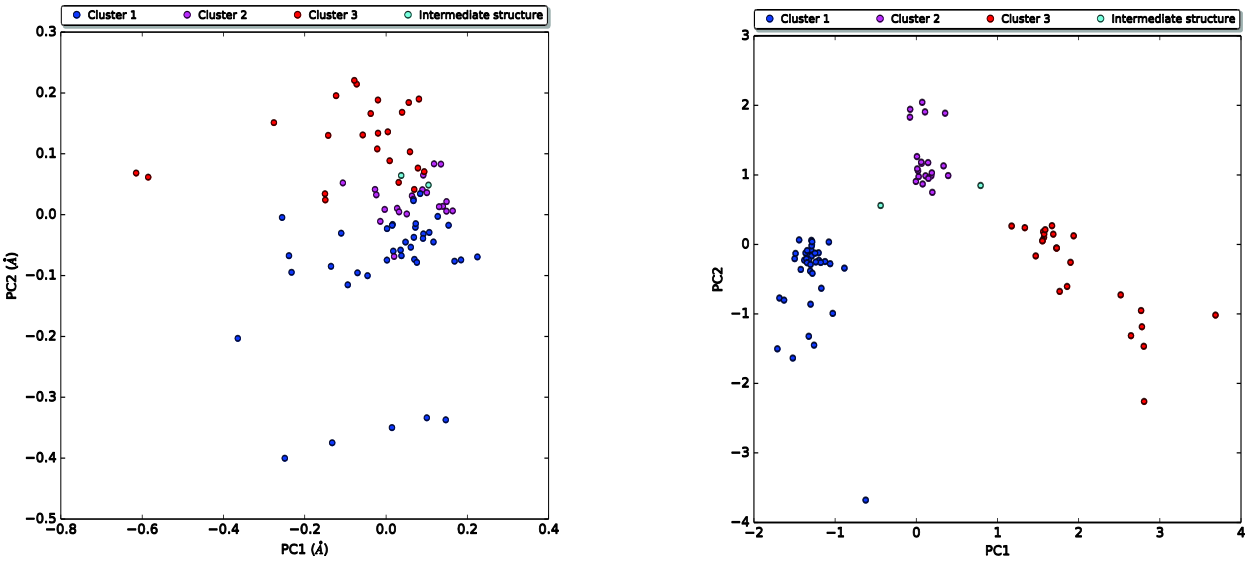

(**A**) (**B**)

Figure 4. cPCA (**A**) and dPCA (**B**) of type A chain PPARγ homodimeric structures coloured according to the clusters observed in the dPCA (**B**).

While the variances defining the principal components derived from atomic (Cartesian) coordinates may be projected back onto the structure for visualization, the sine/cosine transformations of the dPCA preclude this approach. To investigate the angular basis for the clustering observed in dPCA of the final dataset, the angular dispersion of each phi/psi-angle of the backbone was calculated (Figure S4 in the Supporting Information). The six dihedral angles displaying highest angular dispersion (Figure S5) form three pairs of coupled dihedral motion; $\varphi_{Lys358}/\psi_{Lys358}$ located in the loop between helices 6 and 7, $\varphi_{Ser394}/\psi_{Gly395}$ located in the loop between helices 8 and 9 and $\varphi_{Tyr473}/\psi_{Lys474}$ located in helix 12. Of these, $\varphi_{Lys358}/\psi_{Lys358}$ separates Cluster 1 from Clusters 2 and 3, by a near 180° flip of the carbonyl group of Lys358. This in turn impacts on the orientation of its alkylamine side chain, but not that of its neighbour, Arg357 (as is discussed below). Furthermore, it appears to significantly shift the position of the pyrrolidine ring of Pro359 and to have a minor effect on the position of the phenyl ring of Phe360 (Figures S6 and S7). $\varphi_{Tyr473}/\psi_{Lys474}$ separates Clusters 1 and 2 from Cluster 3 by a flip of the Tyr473 carbonyl. Most notably this leads to a reorientation of the end of helix 12, observed in the distinct positions of the Lys474 carbonyls of the members of Cluster 3, compared to Clusters 1 and 2. The orientations of the Lys474 carbonyl groups also vary more between the members of Cluster 3, than among the members of Clusters 1 and 2. This, in turn, appears to change the protrusion of the aminoalkyl side chain of Lys474. Such apparent effects were not observed with respect to Ile472 or Glu471, the latter of which is involved in the binding of coactivator peptides[10,61,62] (Figures S8 and S9). Finally, $\varphi_{Ser394}/\psi_{Gly395}$ separates out a subcluster (Cluster 4) from Cluster 3, which with respect to the two previous described dihedral pairs, is part of Cluster 3. The dihedral pair $\varphi_{Ser394}/\psi_{Gly395}$ is located in close proximity to the heterodimer interface and may thus influence the interaction of PPARγ with RXR. The neighbouring residue Asp396

shows two distinct orientations and appears to form an ionic bond to Arg443 on helix 10 in one of these. With respect to the cluster defined by $\varphi_{Ser394}/\psi_{Gly395}$, the most prominent orientations of Asp396/Arg443 among its members breaks this contact, and allows Arg443 to point in the direction of the C-terminal end of helix 12 (Figures S10 and S11). In summary, the dPCA clusters observed in the final dataset describe structural changes in areas that are plausibly related to PPARγ transcriptional regulation.

The dihedral pair containing the angle showing the largest angular dispersion, ψ_{Lys358}, merits further discussion. Lys358 is flanked by Arg357, Pro359 and Phe360. Of these, Arg357 can form an ionic bridge to Glu460, located near the end of helix 11. This ionic network also involves Glu276 on helix 3. This interaction pattern is present in many of the type A chains, but not in the type B chains (e.g. in apo-PPARγ, see Figure S12 in the Supporting Information). Furthermore, the stabilization of the end of helix 11 is observed to vary markedly between apo-PPARγ and complexes with partial agonists and full agonists.[11,63] These observations led us to hypothesize that the strength of the ionic interaction between Arg357 and Glu460 could correlate with the stability of helix 12. Indeed others have found that this ionic network is critical to the low transactivation capacity of the human PPARγ mutant Phe360Leu, found in persons suffering from familial partial lipodystrophy.[64] Therefore, the correlation of the distances between Arg357 and Glu460, and the distributions along PC1 – 2 was evaluated. For this, the C_α-carbons were preferred over the O- and N-atoms that directly take part in the ionic interaction, as the former are more likely to reflect the effects on the PPARγ backbone and on the overall compactness of this part of the PPARy structure. In this context it is interesting to note that the opening of the LBP circumscribed by the start of helix 3, helix 2', the helix 6 -7 loop and the end of helix 11 has been indicated as a possible ligand exit pathway in MD simulations.[65] Consequently, a short

distance between Arg357 and Glu460 may be regarded as corresponding to a tightly bound ligand. As seen in Figure 5A, the distribution observed along cPC1 correlated moderately with the Arg357 - Glu460 distance, placing the structures with the shortest distances towards the right side of the distribution (cPC1 > 0). In the dPCA, on the other hand, this trend was not observed and all three clusters are populated by structures with both long and short Arg357 – Glu460 distances (Figure 6B).

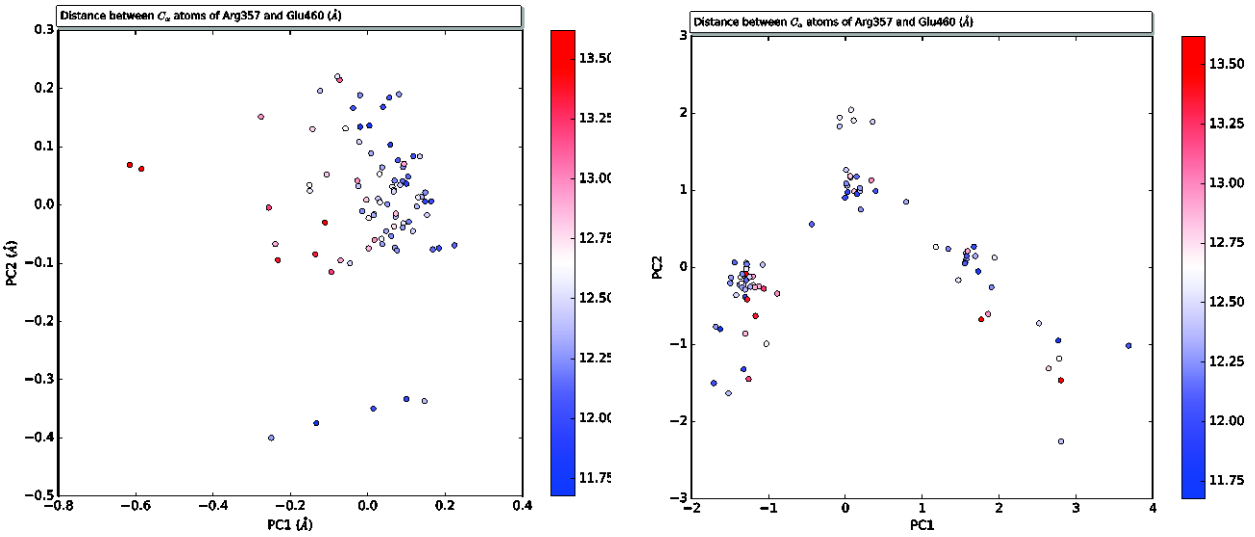

(**A**) (**B**)

Figure 5. cPCA (**A**) and dPCA (**B**) of type A chain PPARγ homodimeric structures coloured according to the distance between the C_α-carbons of Arg357, in the loop between helix 6 and 7, and Glu460, near the end of helix 11. The distance measurement from PDB ID: 4xta was excluded based on the apparent structural inconsistencies in the modelling of the proline ring of Pro359.

X-ray crystallographic studies of PPARγ in complex with ligands have been instrumental to the rational development of new PPARγ modulators. These studies have identified residues that appear to play key roles in the stabilization of the receptor and in particular, of helix 12. To further investigate the relationship of the trend in the Arg357 – Glu460 distance, observed in along cPC1 (Figure 5A), with a stabilization of helix 12 by the ligand(s) of each structure, we evaluated the correlation of the distributions with presence of an interaction between the ligand and Tyr473, and the observed B-factors of Tyr473. In the first pair of plots from the cPCA and dPCA (Figure 6, A and B), the points are coloured according to whether the ligands display an interaction with Tyr473 (defined as an interatomic distance of < 3.5 Å between the nearest heavy atoms). In the second pair of plots (Figure 6, C and D), the B-factors of the heavy atoms of Tyr473 are used to colour the datapoint belonging to each structure. The combination of an interaction with Tyr473, with a lowering of its B-factors, may be interpreted as a stabilizing interaction. It is however prudent to consider that a ligand may stabilize helix 12 in a position that is not conducive to transcriptional induction. In the cPCA plots (Figure 6, A and C), a stabilization of Tyr473 weakly correlates to cPC1, and to some degree with cPC2. This can be seen as a higher degree of structures with ligands interacting with Tyr473 towards the lower right side of the largest cluster in Figure 6A (cPC1 > 0), and as a decrease in the B-factors of Tyr473 when moving from the upper left corner (cPC1 < 0, cPC2 > 0) to the lower right corner (cPC1 > 0, cPC2 < 0) of Figure 6C. Interestingly, as several of the structures that display lower B-factors, located towards the lower right side of the largest cluster in Figure 6C, do not contain ligands that appear to contact Tyr473, it is possible that the distribution along cPC1 also reflects an allosteric stabilization of helix 12. Similar correlations were not evident in the dPCA (Figure 6, B and D), although the leftmost cluster in Figure 6D (Cluster 1) appears to contain the highest

number of structures in which Tyr473 displays low B-factors. Similar trends with regards to ligand interactions with residues in the β-sheet region (residues 247 – 249 and 338 – 349) and their observed B-factors, were not observed (Figure S13 in the Supporting Information). It is however worthy of note that several of the larger ligands whose head groups bind in the vicinity of helix 12, have tail moieties that extend into the Ω-pocket and contact the β-sheet region. This double interaction pattern could make the latter analysis described here less tractable. In summary, the general similarity of cPCA distribution coloured by the B-factors of Tyr473 with that coloured by the Arg357 – Glu460 distance is an indications that the cPCA is capable of separating the structures based on parameters related to the stability of helix 12.

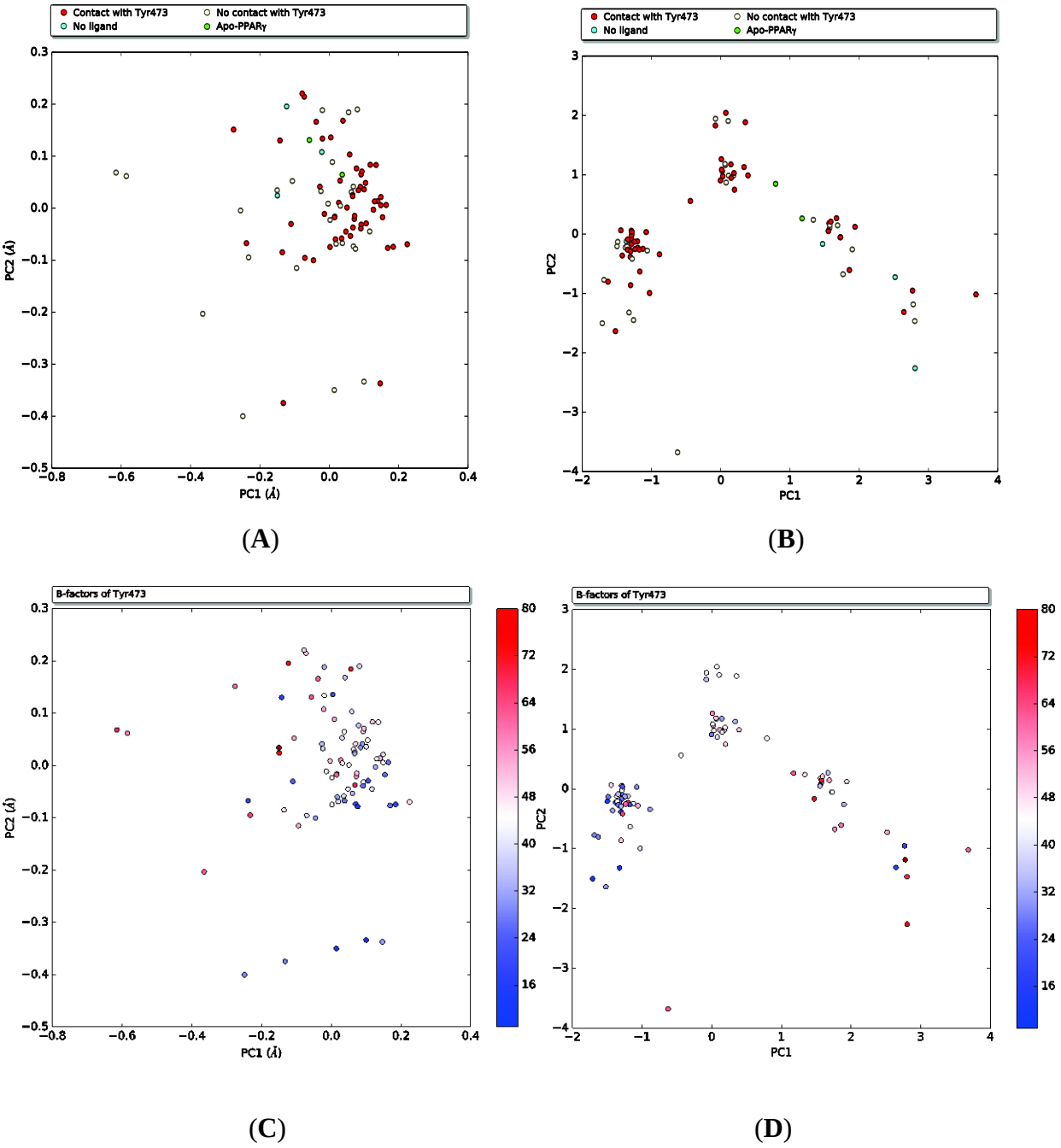

Figure 6. *Top:* cPCA (**A**) and dPCA (**B**) of type A chain PPARγ homodimeric structures coloured according to the close contact of their ligands with Tyr473 (3.5 Å cutoff). *Bottom:* cPCA (**C**) and dPCA (**D**) of type A chain PPARγ homodimeric structures coloured according to the B-factors of Tyr473 in helix 12.

To investigate in more detail the distribution of the homodimeric type A chains along PC1 – 2, the structures were coloured according to a chemical classification of their ligands. Due to the structural diversity of the ligands in the analyzed structures, only 7 classes containing ≥ 3 structures can be distinguished. In the cPCA (Figure 7A), the location of the glitazones and glitazars towards the right of the distribution is coherent with an increasing stability of helix 12 (cPC > 0). Furthermore, there are distinguishable clusterings of the 2-aryloxy-3-arylpropanoic acids, serotonin and its metabolites and the amorfrutins. The fatty acids and their metabolites form a slighly more elongated cluster (Figure 7) It is also noteworthy that the covalently bound ligands (many of which are oxo-fatty acids) are located fairly close to each other (points with red outlines). The last class is made up of ligands that are not structurally related, but that induce a higher maximum transcriptional activation of chimeric PPARγ reporter assays than rosiglitazone (**1**, Figure 2). Interestingly, the members of this class are not located further to the right than the glitazones/glitazars. This is an indication that the distribution along cPC1 may not linearly reflect the transcriptional activation by a given ligand. In the dPCA, the 2-aryloxy-3-arylpropanoic acids exclusively occupy the rightmost cluster (Cluster 3), while none of the covalently bound ligands nor any of the fatty acids are present in this cluster. The amorfrutins, on the other hand, all reside in Cluster 1. The glitazones/glitazars do not display any particular preference for any of the clusters.

In the same vein, the structures were coloured according to the available data on the ability of their cocrystallized ligands to inhibit the Cdk5-mediated phosphorylation of Ser245 (Ser273), denoted “pSer245” in the plots. The ligands reported to inhibit this phosphorylation are represented both among classical (full) agonists, as well as among the partial agonists/non-agonists (Table S1 in the Supporting Information). While the distributions along cPC1 and cPC2

did not provide a distinct clustering of the structures with these ligands (Figure 7, B and C), there is however a tendency for cPC1 to separate the structures of non-TZD ligands that inhibit Ser245 (Ser273) phosphorylation (yellow points) from the TZD ligands with the same ability (orange points). No such trend was observed in the dPCA (Figure 4B).

Having established that the distribution of the structures along cPC1 is to some degree related to the stability of helix 12, we evaluated whether cPC1 could reflect the transcriptional activation by each ligand compared to rosiglitazone (**1**). As a measure of this, we used the reported percentage of maximal activation by each ligand in chimeric PPARγ reporter assays (commonly GAL4-PPARγ hybrid acting on luciferase reporter constructs), including only series of ligands assayed in the same report. As seen in Figure 8, several of the ligand series display internally coherent increases in transcriptional activation relative to their distribution along cPC1, the series with the amorfrutins being a notable exception. It also apparent that the levels of transcriptional activation are not comparable between each ligand series. As mentioned above in connection with the positions along cPC1 of agonists that are stronger transcriptional activators than rosiglitazone (**1**), this finding supports the notion that cPC1 does not directly reflect the capacity of the PPARγ-ligand complexes for transcriptional activation.

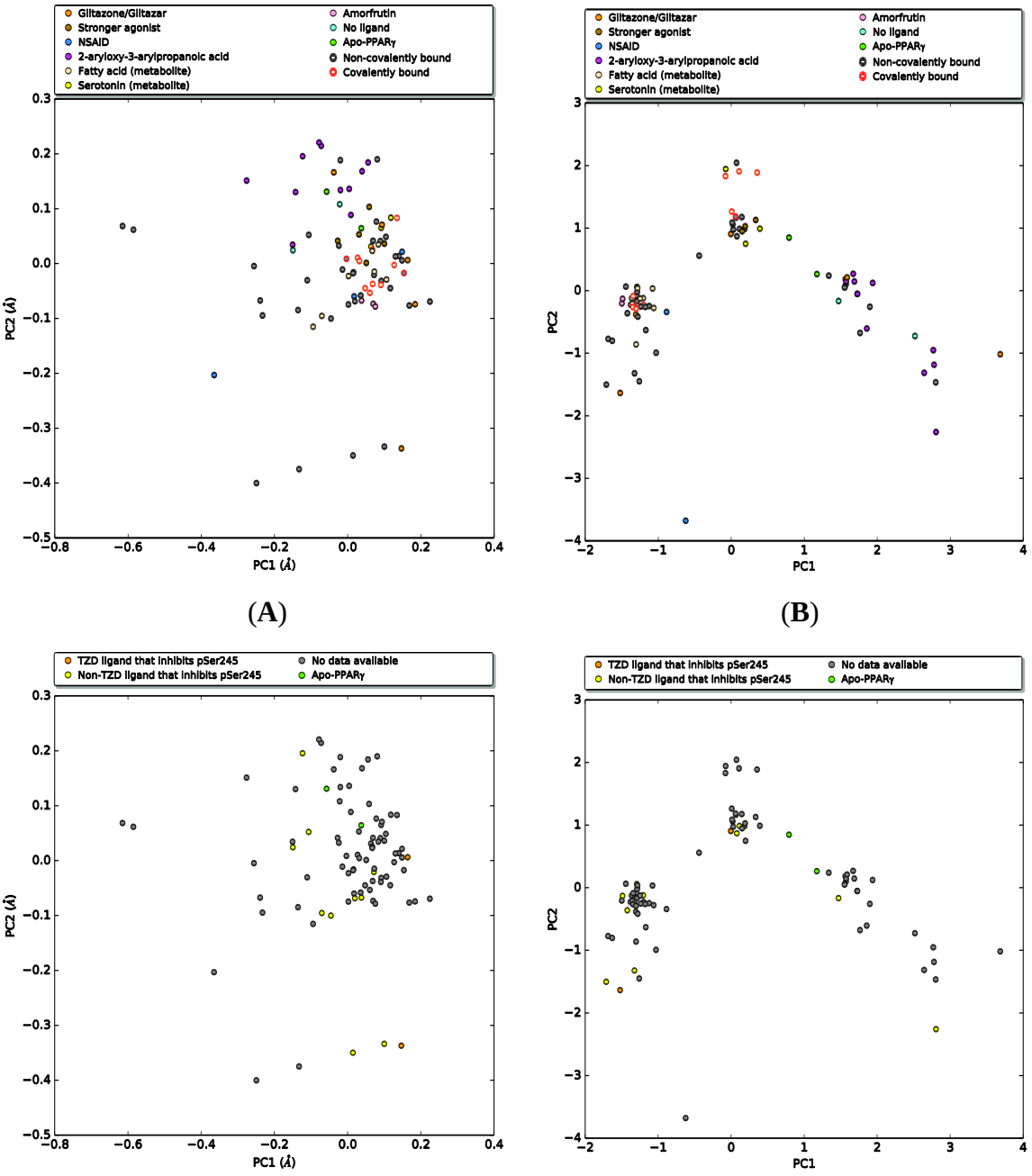

Figure 7. *Top:* cPCA (**A**) and dPCA (**B**) of type A chain PPARγ homodimeric structures coloured according to a chemical classification of their ligands. *Bottom:* cPCA (**C**) and dPCA (**D**) of type A chain PPARγ homodimeric structures coloured according to the reported ability of the ligands to inhibit phosphorylation of Ser245 (Ser273) (Table S1 in the Supporting Information).

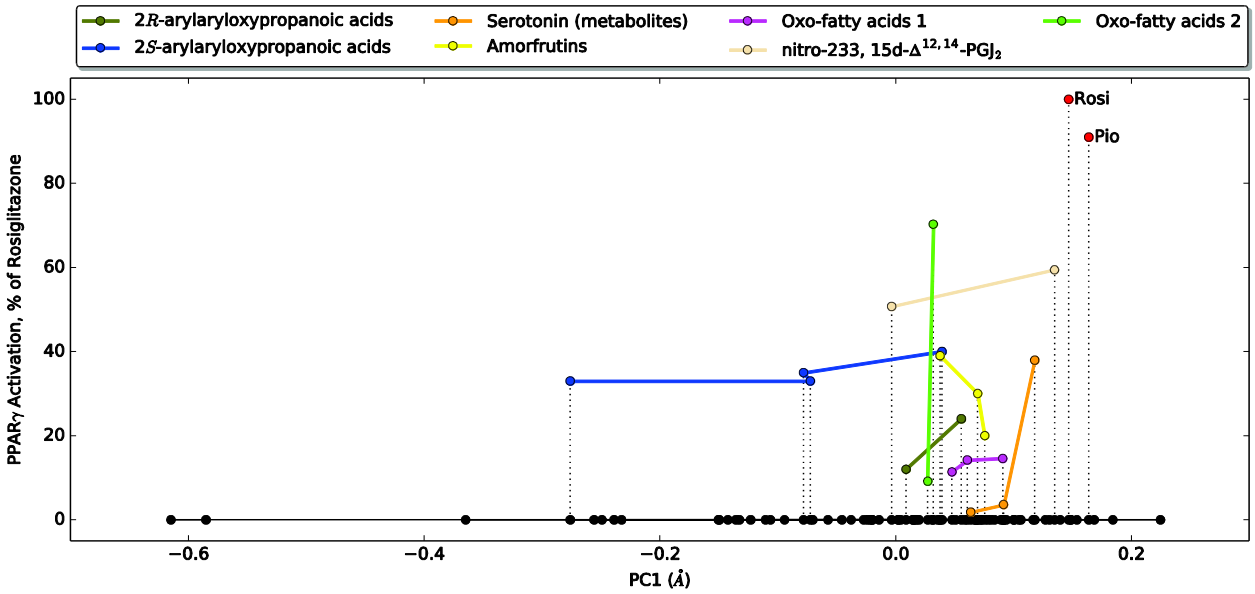

Figure 8. Evaluation of the correlation between the transcriptional activation of the ligands compared to rosiglitazone (**1**, Figure 2) and their position in the distribution along cPC1.

Conclusions

Principal component analyses of the atomic coordinates and dihedral angles of PPARγ in complex with ligands have been demonstrated. The results from the cPCA indicate trends among the structures in the final dataset that correlate with a stabilization of helix 12 and with the distance between Arg357 and Glu460. In drug discovery programs targeting PPARγ, the focus has shifted from of helix 12-stabilizing classical agonists, to partial- and non-agonistic ligands with alternative binding modes and more desirable pharmacological properties. Our findings should be useful to medicinal- and computational chemists working towards the development of new such ligands. In this vein, the structures in which helix 12 is not found to be stabilized by the ligand, possibly neither directly nor allosterically, may be used as starting points for virtual screening campaigns or MD studies aiming to elucidate structure-activity relationships in the PPARγ Ω-pocket. Furthermore, dPCA of type A chains from PPARγ homodimers produces an apparent tripart clustering of the holo-PPARγ structures when projected along dPC1 - 2. To determine the physical relevance of the observed clustering, in the context of the conformational spaces populated by PPARγ in the crystal phase and in solution, the application of dPCA to mesoscale datasets of PPARγ structural dynamics, as observed with NMR or MD, would be of immediate interest.

Acknowledgements

This study was supported by Biocenter Finland/DDCB (TL). The European Cooperation in the field of Scientific and Technical Research (COST), Action CM 0804, is gratefully acknowledged for its generous financial support to Å.K. in the matters of two short-term science missions (STSMs) to the School of Pharmacy, UEF, Kuopio, Finland. The School of Pharmacy, University of Oslo and MLS^{UIO} are also acknowledged for their financial support.

References

1. Ahmadian M, Suh JM, Hah N, Liddle C, Atkins AR, Downes M, Evans RM. PPARγ signaling and metabolism: the good, the bad and the future. Nature Medicine. 2013;99(5):557–566.

2. Kiss-Tóth É, Rőszer T. PPARγ in Kidney Physiology and Pathophysiology. PPAR Research. 2008;2008:1–9.

3. Lecka-Czernik B. PPARγ, an essential regulator of bone mass: Metabolic and molecular cues. IBMS BoneKEy. 2010;7(5):171–181.

4. Quintanilla RA, Utreras E, Cabezas-Opazo FA. Role of PPARγ in the Differentiation and Function of Neurons. PPAR Research. 2014;2014:9.

5. Choi JH, Banks AS, Estall JL, Kajimura S, Boström P, Laznik D, Ruas JL, Chalmers MJ, Kamenecka TM, Blüher M, et al. Anti-diabetic drugs inhibit obesity-linked phosphorylation of PPARγ by Cdk5. Nature. 2010;466(7305):451–456.

6. Nissen SE. The rise and fall of rosiglitazone. European Heart Journal. 2010;31(7):773–776.

7. Aubert RE, Herrera V, Chen W, Haffner SM, Pendergrass M. Rosiglitazone and pioglitazone increase fracture risk in women and men with type 2 diabetes. Diabetes, Obesity and Metabolism. 2010;12(8):716–721.

8. Hughes TS, Chalmers MJ, Novick S, Kuruvilla DS, Chang MR, Kamenecka TM, Rance M, Johnson BA, Burris TP, Griffin PR, et al. Ligand and Receptor Dynamics Contribute to the Mechanism of Graded PPARγ Agonism. Structure. 2012;20(1):139–150.

9. Hughes TS, Giri PK, de Vera IMS, Marciano DP, Kuruvilla DS, Shin Y, Blayo A-L, Kamenecka TM, Burris TP, Griffin PR, et al. An alternate binding site for PPARγ ligands. Nature Communications. 2014;5:1–13.

10. Nolte RT, Wisely GB, Westin S, Cobb JE, Lambert MH, Kurokawa R, Rosenfeld MG, Willson TM, Glass CK, Milburn MV. Ligand binding and co-activator assembly of the peroxisome proliferator-activated receptor-γ. Nature. 1998;395(6698):137–143.

11. Bruning JB, Chalmers MJ, Prasad S, Busby SA, Kamenecka TM, He Y, Nettles KW, Griffin PR. Partial Agonists Activate PPARγ Using a Helix 12 Independent Mechanism. Structure. 2007;15(10):1258–1271.

12. Marciano DP, Kuruvilla DS, Boregowda SV, Asteian A, Hughes TS, Garcia-Ordonez R, Corzo CA, Khan TM, Novick SJ, Park H, et al. Pharmacological repression of PPARγ promotes osteogenesis. Nature Communications. 2015;6:7443.

13. Choi JH, Banks AS, Kamenecka TM, Busby SA, Chalmers MJ, Kumar N, Kuruvilla DS, Shin Y, He Y, Bruning JB, et al. Antidiabetic actions of a non-agonist PPARγ ligand blocking Cdk5-mediated phosphorylation. Nature. 2011;477(7365):477–481.

14. Ho BK, Gruswitz F. HOLLOW: Generating Accurate Representations of Channel and Interior Surfaces in Molecular Structures. BMC Structural Biology. 2008;8(1):49.

15. The PyMOL Molecular Graphics System 1.3r1. Schrödinger LLC; 2010.

16. Waku T, Shiraki T, Oyama T, Fujimoto Y, Maebara K, Kamiya N, Jingami H, Morikawa K. Structural Insight into PPARγ Activation Through Covalent Modification with Endogenous Fatty Acids. Journal of Molecular Biology. 2009;385(1):188–199.

17. Waku T, Shiraki T, Oyama T, Maebara K, Nakamori R, Morikawa K. The nuclear receptor PPARγ individually responds to serotonin- and fatty acid-metabolites. EMBO J. 2010;29(19):3395–3407.

18. Weidner C, de Groot JC, Prasad A, Freiwald A, Quedenau C, Kliem M, Witzke A, Kodelja V, Han C-T, Giegold S. Amorfrutins are potent antidiabetic dietary natural products. Proceedings of the National Academy of Sciences. 2012;109(19):7257–7262.

19. de Groot JC, Weidner C, Krausze J, Kawamoto K, Schroeder FC, Sauer S, Büssow K. Structural Characterization of Amorfrutins Bound to the Peroxisome Proliferator-Activated Receptor γ. Journal of Medicinal Chemistry. 2013;56(4):1535–1543.

20. Calleri E, Pochetti G, Dossou KSS, Laghezza A, Montanari R, Capelli D, Prada E, Loiodice F, Massolini G, Bernier M, et al. Resveratrol and Its Metabolites Bind to PPARs. ChemBioChem. 2014;15(8):1154–1160.

21. Puhl AC, Milton FA, Cvoro A, Sieglaff DH, Campos JC, Bernardes A, Filgueira CS, Lindemann JL, Deng T, Neves FA, et al. Mechanisms of peroxisome proliferator activated receptor γ regulation by non-steroidal anti-inflammatory drugs. Nuclear Receptor Signaling. 2015;13:e004.

22. Johnson BA, Wilson EM, Li Y, Moller DE, Smith RG, Zhou G. Ligand-induced stabilization of PPARγ monitored by NMR spectroscopy: implications for nuclear receptor activation. Journal of Molecular Biology. 2000;298(2):187–194.

37 R. Hartl, Berechnung der NMR-Struktur der PPARgamma-LBD und Hochdruck-NMR-Messungen an HPr I14A, Ph.D. Thesis, University of Regensburg, Germany, 2008.

24. Lemkul JA, Lewis SN, Bassaganya-Riera J, Bevan DR. Phosphorylation of PPARγ Affects the Collective Motions of the PPARγ-RXRα-DNA Complex Uversky VN, editor. PLOS ONE. 2015;10(5):e0123984.

25. Nettles KW. Insights into PPARγ from structures with endogenous and covalently bound ligands. Nature structural & molecular biology. 2008;15(9):893–895.

26. Ricci CG, Silveira RL, Rivalta I, Batista VS, Skaf MS. Allosteric Pathways in the PPARγ-RXRα nuclear receptor complex. Scientific Reports. 2016;6:19940.

27. Malapaka RRV, Khoo S, Zhang J, Choi JH, Zhou XE, Xu Y, Gong Y, Li J, Yong E-L, Chalmers MJ, et al. Identification and Mechanism of 10-Carbon Fatty Acid as Modulating Ligand of Peroxisome Proliferator-activated Receptors. Journal of Biological Chemistry. 2011;287(1):183–195.

28. Wakabayashi K, Hayashi S, Matsui Y, Matsumoto T, Furukawa A, Kuroha M, Tanaka N, Inaba T, Kanda S, Tanaka J. Pharmacology and in Vitro Profiling of a Novel Peroxisome Proliferator-Activated Receptor γ Ligand, Cerco-A. Biological and Pharmaceutical Bulletin. 2011;34(7):1094–1104.

29. Zhou G, Cummings R, Li Y, Mitra S, Wilkinson HA, Elbrecht A, Hermes JD, Schaeffer JM, Smith RG, Moller DE. Nuclear Receptors Have Distinct Affinities for Coactivators: Characterization by Fluorescence Resonance Energy Transfer. Molecular Endocrinology. 1998;12(10):1594–1604.

30. Weikl TR, Paul F. Conformational selection in protein binding and function. Protein Science. 2014;23(11):1508–1518.

31. Meireles L, Gur M, Bakan A, Bahar I. Pre-existing soft modes of motion uniquely defined by native contact topology facilitate ligand binding to proteins. Protein Science. 2011;20(10):1645–1658.

32. Batista MRB, Martínez L. Conformational Diversity of the Helix 12 of the Ligand Binding Domain of PPARγ and Functional Implications. The Journal of Physical Chemistry B. 2015;119(50):15418–15429.

33. Jolliffe IT. Introduction. In: Principal Component Analysis. Springer New York; 2002. p. 1–9. (Springer Series in Statistics).

34. Lange OF, Grubmüller H. Full correlation analysis of conformational protein dynamics. Proteins: Structure, Function, and Bioinformatics. 2007;70(4):1294–1312.

35. Amadei A, Linssen ABM, Berendsen HJC. Essential dynamics of proteins. Proteins: Structure, Function, and Bioinformatics. 1993;17(4):412–425.

36. Bakan A, Bahar I. Computational Generation inhibitor-Bound Conformers of P38 Map Kinase and Comparison with Experiments. In: Pacific Symposium on Biocomputing. Vol. 16. World Scientific; 2011. p. 181–192. http://www.worldscientific.com/doi/pdf/10.1142/9789814335058_0020

37. Bakan A, Bahar I. The intrinsic dynamics of enzymes plays a dominant role in determining the structural changes induced upon inhibitor binding. Proceedings of the National Academy of Sciences. 2009;106(34):14349–14354.

38. Yang L, Song G, Carriquiry A, Jernigan RL. Close Correspondence between the Motions from Principal Component Analysis of Multiple HIV-1 Protease Structures and Elastic Network Modes. Structure. 2008;16(2):321–330.

39. Stock G, Jain A, Riccardi L, Nguyen PH. Exploring the Energy Landscape of Small Peptides and Proteins by Molecular Dynamics Simulations. In: Protein and Peptide Folding, Misfolding, and Non-Folding. John Wiley & Sons, Inc.; 2012. p. 55–77.

40. Altis A, Otten M, Nguyen PH, Hegger R, Stock G. Construction of the free energy landscape of biomolecules via dihedral angle principal component analysis. The Journal of Chemical Physics. 2008;128(24):245102.

41. Altis A, Nguyen PH, Hegger R, Stock G. Dihedral angle principal component analysis of molecular dynamics simulations. The Journal of Chemical Physics. 2007;126(24):244111.

42. Mu Y, Nguyen PH, Stock G. Energy landscape of a small peptide revealed by dihedral angle principal component analysis. Proteins: Structure, Function, and Bioinformatics. 2005;58(1):45–52.

43. Sargsyan K, Wright J, Lim C. GeoPCA: a new tool for multivariate analysis of dihedral angles based on principal component geodesics. Nucleic Acids Research. 2012;40(3):e25–e25.

44. Joosten RP, Long F, Murshudov GN, Perrakis A. The *PDB_REDO* server for macromolecular structure model optimization. IUCrJ. 2014;1(4):213–220.

45. Joosten RP, Salzemann J, Bloch V, Stockinger H, Berglund A-C, Blanchet C, Bongcam-Rudloff E, Combet C, Da Costa AL, Deleage G, et al. PDB_REDO: automated re-refinement of X-ray structure models in the PDB. Journal of Applied Crystallography. 2009;42(3):376–384.

46. Berman HM, Westbrook J, Feng Z, Gilliland G, Bhat TN, Weissig H, Shindyalov IN, Bourne PE. The Protein Data Bank. Nucleic Acids Research. 2000;28(1):235–242.

47. Bakan A, Meireles LM, Bahar I. ProDy: Protein Dynamics Inferred from Theory and Experiments. Bioinformatics. 2011;27(11):1575–1577.

48. Humphrey W, Dalke A, Schulten K. VMD – Visual Molecular Dynamics. Journal of Molecular Graphics. 1996;14:33–38.

49. Best RB, Zhu X, Shim J, Lopes PEM, Mittal J, Feig M, MacKerell AD. Optimization of the Additive CHARMM All-Atom Protein Force Field Targeting Improved Sampling of the Backbone ϕ, ψ and Side-Chain $\chi 1$ and $\chi 2$ Dihedral Angles. Journal of Chemical Theory and Computation. 2012;8(9):3257–3273.

50. Glykos NM. Software news and updates carma: A molecular dynamics analysis program. Journal of Computational Chemistry. 2006;27(14):1765–1768.

51. Koukos PI, Glykos NM. Grcarma: A fully automated task-oriented interface for the analysis of molecular dynamics trajectories. Journal of Computational Chemistry. 2013;34(26):2310–2312.

52. Python Reference Manual. https://docs.python.org/2.7/; 2016.

53. Nagy L, Schwabe JWR. Mechanism of the nuclear receptor molecular switch. Trends in Biochemical Sciences. 2004;29(6):317–324.

54. Riepl H, Hartl R, Bauer M, Nar H, Kauschke S, Kalbitzer H, Maurer T. Sequential Backbone Assignment of Peroxisome Proliferator-Activated Receptor-γ Ligand Binding Domain. Journal of Biomolecular NMR. 2005;32(3):259.

55. Ohashi M, Oyama T, Miyachi H. Different structures of the two peroxisome proliferator-activated receptor gamma (PPARγ) ligand-binding domains in homodimeric complex with partial agonist, but not full agonist. Bioorganic & Medicinal Chemistry Letters. 2015;25(13):2639–2644.

56. Yang L-W, Eyal E, Chennubhotla C, Jee J, Gronenborn AM, Bahar I. Insights into Equilibrium Dynamics of Proteins from Comparison of NMR and X-Ray Data with Computational Predictions. Structure. 2007;15(6):741–749.

57. Davis A, Stgallay S, Kleywegt G. Limitations and lessons in the use of X-ray structural information in drug design. Drug Discovery Today. 2008;13(19–20):831–841.

58. Hinsen K. Structural flexibility in proteins: impact of the crystal environment. Bioinformatics. 2008;24(4):521–528.

59. d'Agostino RB. An omnibus test of normality for moderate and large size samples. Biometrika. 1971;58(2):341–348.

60. d'Agostino RB, Pearson ES. Tests for departure from normality. Empirical results for the distributions of b2 and√ b1. Biometrika. 1973;60(3):613–622.

61. Wu Y, Chin WW, Wang Y, Burris TP. Ligand and Coactivator Identity Determines the Requirement of the Charge Clamp for Coactivation of the Peroxisome Proliferator-activated Receptor γ. Journal of Biological Chemistry. 2003;278(10):8637–8644.

62. Walkey CJ, Spiegelman BM. A Functional Peroxisome Proliferator-activated Receptor-γ Ligand-binding Domain Is Not Required for Adipogenesis. Journal of Biological Chemistry. 2008;283(36):24290–24294.

63. Hamuro Y, Coales SJ, Morrow JA, Molnar KS, Tuske SJ, Southern MR, Griffin PR. Hydrogen/deuterium-exchange (H/D-Ex) of PPARγ LBD in the presence of various modulators. Protein Science. 2006;15(8):1883–1892.

64. Lori C, Pasquo A, Montanari R, Capelli D, Consalvi V, Chiaraluce R, Cervoni L, Loiodice F, Laghezza A, Aschi M, et al. Structural basis of the transactivation deficiency of the human PPARγ F360L mutant associated with familial partial lipodystrophy. Acta Crystallographica Section D Biological Crystallography. 2014;70(7):1965–1976.

65. Genest D, Garnier N, Arrault A, Marot C, Morin-Allory L, Genest M. Ligand-escape pathways from the ligand-binding domain of PPARγ receptor as probed by molecular dynamics simulations. European Biophysics Journal. 2008;37(4):369–379.